Journal of Nuclear Materials 425 (2012) 48–53

Contents lists available at SciVerse ScienceDirect

Journal of Nuclear Materials

journal homepage: www.elsevier.com/locate/jnucmat

# In situ study of heavy ion induced radiation damage in NF616 (P92) alloy

Cem Topbasi [a,*], Arthur T. Motta [a,b], Mark A. Kirk [c]

[a] Department of Materials Science and Engineering, Pennsylvania State University, University Park, PA 16802, USA
[b] Department of Mechanical and Nuclear Engineering, Pennsylvania State University, University Park, PA 16802, USA
[c] Materials Science Division, Argonne National Laboratory, Argonne, IL 60439, USA

ARTICLE INFO

*Article history:*
Available online 12 September 2011

ABSTRACT

NF616 is a nominal 9Cr ferritic–martensitic steel that is amongst the primary candidates for cladding and duct applications in the Sodium-Cooled Fast Reactor, one of the Generation IV nuclear energy systems. In this study, an in situ investigation of the microstructure evolution in NF616 under heavy ion irradiation has been conducted. NF616 was irradiated to 8.4 dpa at 50 K and to 7.6 dpa at 473 K with 1 MeV Kr ions. Nano-sized defects first appeared as white dots in dark-field TEM images and their areal density increased until saturation (~6 dpa). Dynamic observations at 50 K and 473 K showed appearance and disappearance of TEM-visible defect clusters under irradiation that continued above saturation dose. Quantitative analysis showed no significant change in the average size (~3–4 nm) and distribution of defect clusters with increasing dose at 50 K and 473 K. These results indicate a cascade-driven process of microstructure evolution under irradiation in these alloys that involves both the formation of TEM-visible defect clusters by various degrees of cascade overlap and cascade induced defect cluster elimination. According to this mechanism, saturation of defect cluster density is reached when the rate of defect cluster formation by overlap is equal to the rate of cluster elimination during irradiation.



## 1. Introduction

The Sodium-Cooled Fast Reactor (SFR) is one of the six Generation IV nuclear energy system concepts considered in the "Generation IV" international forum [1], offering potential for waste minimization, high efficiency and improved economics. However, the higher operational temperature and longer reactor exposure under intense radiation fields brings new challenges for the nuclear fuel cladding and reactor internal materials used in such reactors [1]. The performance of these materials under these demanding conditions may determine the feasibility of the proposed nuclear energy system.

Ferritic–martensitic (F–M) alloys offer high resistance to irradiation-induced void swelling and good thermal properties, such as high thermal conductivity and low thermal expansion [2]. Because of this, F–M alloys are amongst the primary candidate materials for cladding and duct applications in the SFR. NF616 is a third Generation F–M alloy, which was assigned the code P92 in ASTM Standards [3]. NF616 exhibits improved creep-rupture properties compared to HT-9 [4] which makes it a promising candidate for in-core applications in SFR.

Developing predictive models of irradiation induced microstructure evolution in complex F–M alloys requires benchmarking the modeling results against experimental data collected over a wide range of temperatures, to be able to properly assess the model's effectiveness.

However, only a limited number of studies have been performed on the high-dose irradiation behavior of these F–M alloys.

Horsten et al. studied the irradiation behavior of two third Generation F–M alloys, NF616 (nominal 9Cr alloy) and HCM12A (12Cr nominal alloy) [5]. NF616 and HCM12A were irradiated in the core of a high flux reactor up to a target dose of 2.5 dpa at 573 K and 2.0 dpa at 343 K. Results of the Charpy tests conducted on NF616 and HCM12A showed ductile-to-brittle transition temperature shifts of 249 K and 225 K, respectively. In addition, HCM12A exhibited more hardening than NF616 [5].

Allen et al. performed heavy-ion (5.0 MeV Ni) and 2 MeV proton irradiation of HCM12A [6]. Proton irradiation was conducted to doses of 3, 7 and 10 dpa at 673 K and to a dose of 3 dpa at 773 K. Hardness measurements performed on the alloy irradiated at 673 K showed an increase of up to 70% in hardness saturating around 5 dpa [6]. On the other hand, a relatively small increase in hardness was reported for HCM12A irradiated at 773 K to 7 dpa. The hardening of proton irradiated HCM12A was mainly attributed to the formation of irradiation-induced precipitates and loops [6]. The Ni ion irradiation was performed at 773 K to doses of 5 and 50 dpa. Microstructural analysis performed on the Ni irradiated alloys showed no significant change in microstructure, although radiation induced loops, voids and precipitates were observed in the proton irradiated HCM12A alloy at 773 K [6].

* Corresponding author. Tel.: +1 814 865 9709; fax: +1 814 865 8499.
*E-mail address:* cemt@psu.edu (C. Topbasi).

0022-3115/$ - see front matter © 2011 Elsevier B.V. All rights reserved.
doi:10.1016/j.jnucmat.2011.08.046

**Table 1**
Composition of NF616 in wt.%.

| C | Cr | Fe | Si | P | S | V | Mn | Ni | Nb | Mo | W | Al |
|---|---|---|---|---|---|---|---|---|---|---|---|---|
| 0.11 | 8.82 | Bal. | 0.1 | 0.01 | 0.003 | 0.19 | 0.45 | 0.17 | 0.06 | 0.47 | 1.87 | 0.005 |

Irradiation-induced hardening can be caused by the formation of point defects, defect clusters, loops, and second phase particles under irradiation [5,6]. Thus, a systematic investigation of microstructure evolution of these complex alloys at various temperatures in a wide dose range is needed.

In this study, the microstructure evolution in NF616 alloy under heavy ion irradiation is investigated in situ using the Intermediate Voltage Electron Microscope (IVEM) at Argonne National Laboratory. The in situ technique allows observing the damage evolution as it develops under irradiation. The irradiation-induced defect concentration and size distribution can be studied as a function of dose and temperature, which can be controlled precisely. In addition, the stability of the initial microstructure and the interaction of defects with each other and with pre-existing microstructure under ion irradiation can be examined. Heavy ion irradiation offers high displacement rates and there is no activation of the sample after irradiation [7,8].

## 2. Experiment

The NF616 alloy investigated in this study was provided by Japan Atomic Energy Agency. NF616 was normalized at 1343 K for 1 h, air cooled, then tempered at 1043 K for 2 h and air cooled. The chemical composition of the alloy is given in Table 1.

The microstructure of as fabricated NF616 was characterized by optical microscopy, scanning electron microscopy (SEM) and transmission electron microscopy (TEM). TEM samples were prepared by electropolishing in 5% $HClO_4$ and 95% $CH_3OH$ solution cooled down to 233 K. Samples were prepared for optical and scanning electron microscopy using the etchant with the composition: 45% HCl, 20% $HNO_3$ and 35% $H_2O$.

In situ ion irradiations of NF616 were conducted at the Argonne IVEM-Tandem Facility which is a Hitachi H-9000NAR TEM interfaced with a 2 MeV ion accelerator and a 0.65 MeV ion implanter [9]. The electron-thin NF616 samples were irradiated with 1 MeV Kr ions under a typical flux of $0.5 \times 10^{12}$ $cm^{-2}$ $s^{-1}$. The doses in displacements per atom (dpa) were calculated using the SRIM code, using a displacement energy of 40 eV for Fe and Cr and 28 eV for C [10]. The material was irradiated to 8.4 dpa at 50 K and to 7.6 dpa at 473 K. The sample temperature was measured using a thermocouple attached to the specimen cup and did not vary by more than 1 K. The microscope was operated at 200 keV so no damage is expected from the electron beam. The vacuum was better than $10^{-7}$ torr, so that no sample degradation was seen during

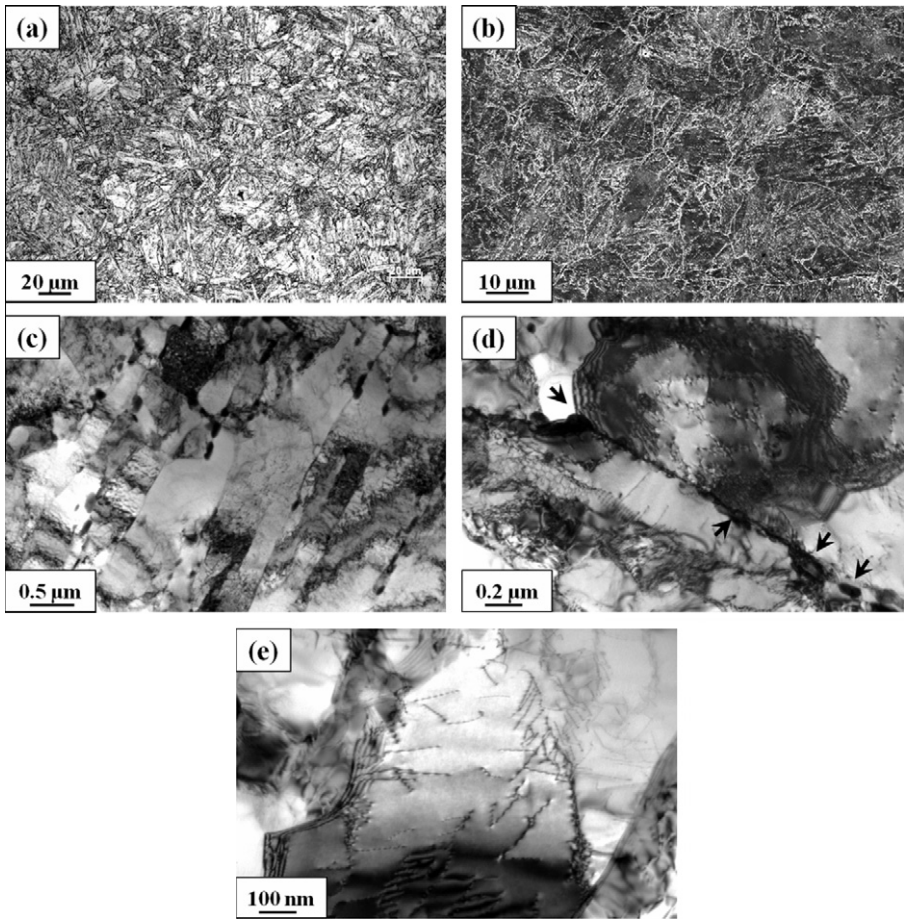


**Fig. 1.** (a) Optical microscopy image of NF616 showing the tempered martensite microstructure. (b) Secondary electron SEM image of prior-austenite grains and the lath structure. (c) Bright field TEM image of elongated lath structure inside prior-austenite grains. (d) Bright field TEM image of a prior-austenite grain boundary decorated with precipitates (precipitates are marked with arrows). (e) Bright field TEM image of the dislocation structure in a weakly recovered lath.

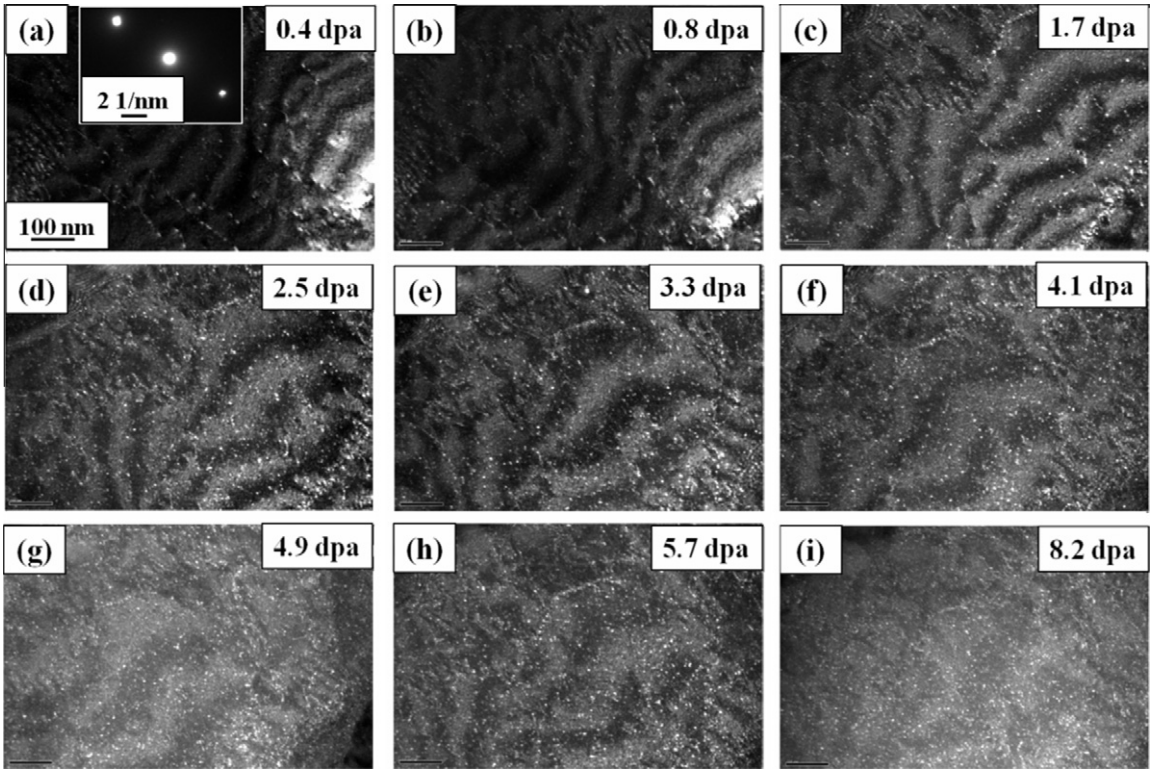


**Fig. 2.** DF TEM images of microstructure evolution of NF616 under 1 MeV Kr Irradiation at 50 K.

irradiation. In the course of the irradiation, specific areas were identified and followed throughout the experiment and irradiation was paused frequently to perform microscopy. Dark-field (DF) TEM images were recorded at regular dose intervals. Defect clusters were counted and measured from the DF TEM images by eye. The defect cluster size was taken as the maximum dimension of the defects on DF TEM images. Occasionally, when the defect contrast was such that defect identification was uncertain, the feature was counted as 1/2 defect [7]. The error bars shown in the defect densities below relate directly to this uncertainty in defect identification.

## 3. Results and discussion

### 3.1. Microstructure

The microstructure of as-fabricated NF616 alloy after the normalization and tempering treatment is shown in Fig. 1. Fig. 1a shows the optical microscopy image of the typical tempered martensite structure of NF616 at room temperature. Fig. 1b shows the secondary electron SEM image, which reveals the prior-austenite grains and the lath structure within. Fig. 1c shows the bright-field TEM image of the elongated laths that form ferrite grains after tempering. Carbide precipitation is observed at lath boundaries and at prior-austenite grain boundaries, with larger precipitates seen at prior-austenite grain boundaries, as shown in Fig. 1d. Laths exhibit a high dislocation density with significant variability between laths. Occasionally, dislocation networks splits the laths and form sub-grain boundaries, as shown in Fig. 1e. The accumulation of irradiation-induced defects was followed within this fine grain structure with high dislocation density. Great care had to be taken to consistently adjust the imaging conditions because of sample magnetism.

### 3.2. Irradiation induced damage evolution

The results of the 1 MeV Kr irradiation of NF616 at 50 K and 473 K are reported in this section. Irradiation-induced defect clusters appear as white dots in the DF TEM images taken in two-beam diffraction conditions. Defects smaller than ~2 nm are below the resolution limit of TEM.

Figs. 2 and 3 show a sequence of two-beam DF TEM images of the specific areas followed throughout the irradiation at 50 K and 473 K, respectively. DF TEM images were captured using 110-type $g$ vectors (Inset of Figs. 2a and 3a) to enable direct comparison. Pre-existing dislocation network was present in the grains monitored under irradiation at 50 K and 473 K, as shown in Figs. 2a and 3a. Note that at 50 K, the first DF TEM image was recorded at 0.4 dpa due to a change in the local diffraction conditions from the beginning of irradiation.

In both irradiations, the overall concentration of visible defects increased steadily with dose until it reached saturation. The sequences of micrographs shown in Figs. 2 and 3 show an increase in the areal number density of defect clusters with increasing dose. The number density appears to saturate around ~6 dpa at 50 K and 473 K, as quantified below. Dynamic observations revealed that individual defect clusters appeared and disappeared during irradiation, both at 50 K and 473 K. This dynamic appearance and disappearance of defect clusters continued beyond the saturation dose.

Fig. 2a, taken at 0.4 dpa, already shows a relatively high density of irradiation-induced defect clusters in the form of white dots. This indicates that at 50 K the accumulation of defects started below 0.4 dpa. In contrast, defect accumulation initiated between 0.5 and 0.8 dpa at 473 K (Fig. 3). The dose for the start of the observations of defect clusters at 473 K could be related to a cascade overlap mechanism, as discussed below. No resolvable loops, voids or irradiation-induced precipitates were observed during either irradiation. Also, no interaction of the irradiation induced defects with

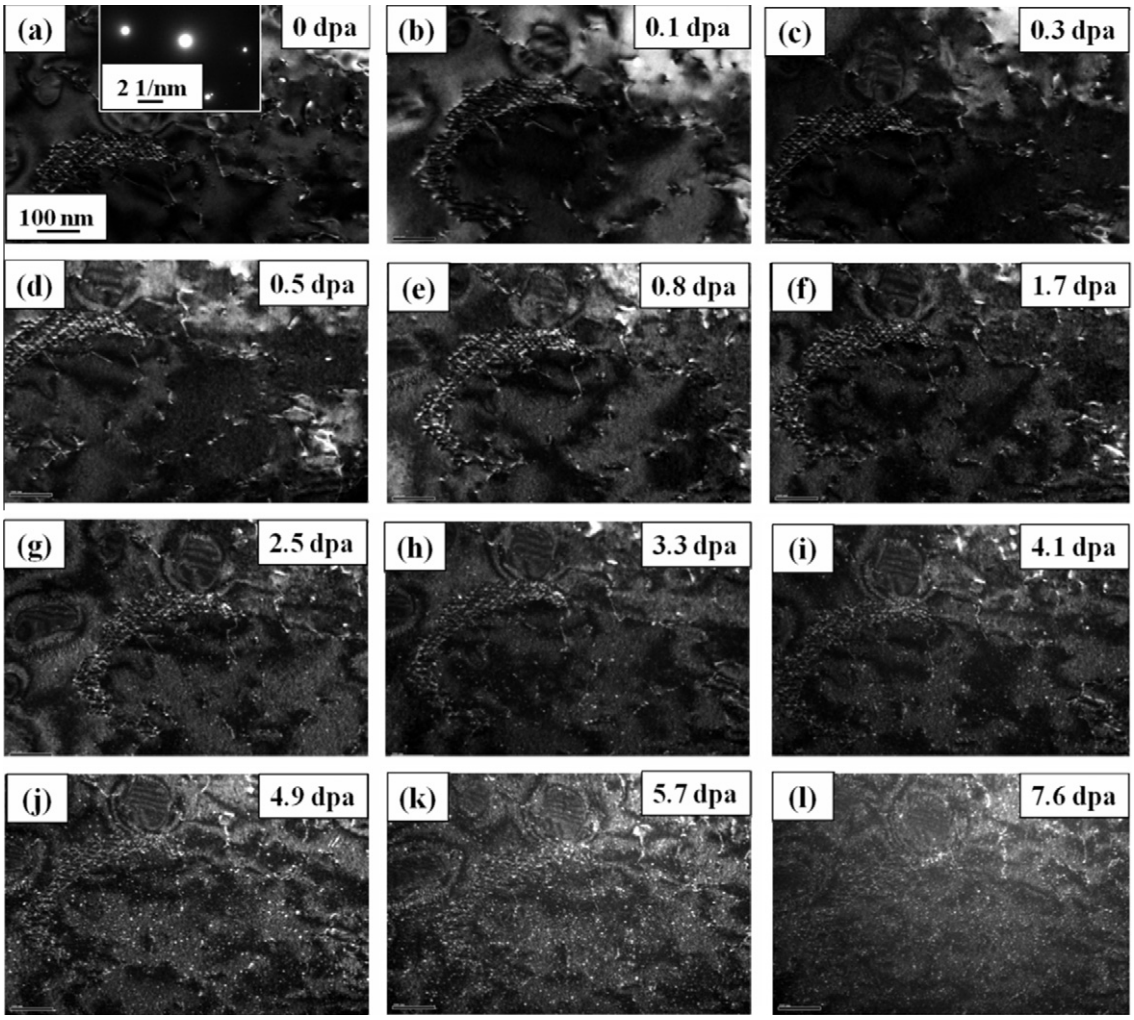


**Fig. 3.** DF TEM images of microstructure evolution of NF616 under 1 MeV Kr Irradiation at 473 K.

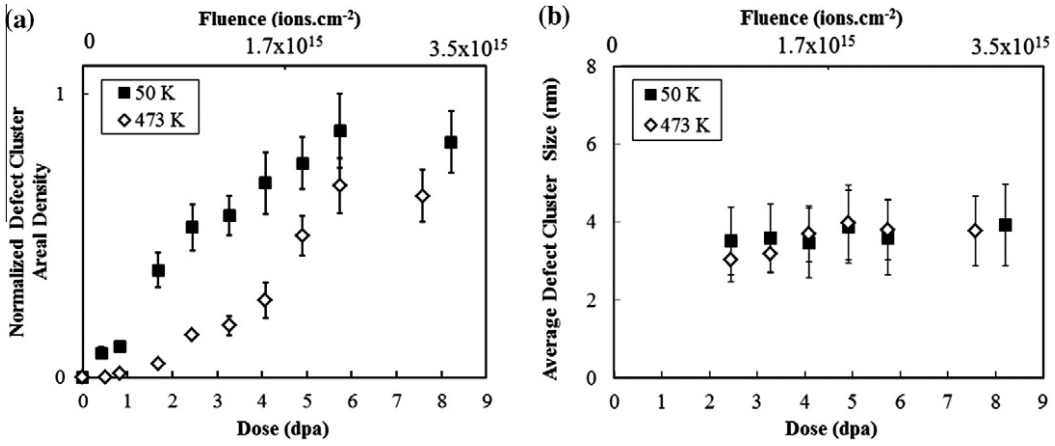


**Fig. 4.** (a) Normalized defect cluster areal density of NF616 as a function of dose at 50 K and 473 K. (b) Average defect cluster size of NF616 as a function of dose at 50 K and 473 K.

the pre-existing microstructure (dislocation network, grain boundaries) in the form of denuded zones, or dislocation climb was observed during the irradiation.

Fig. 4a shows the measured and normalized defect cluster areal density at 50 K and 473 K as a function of dose. The defect cluster density is normalized to the highest value obtained (5.5 dpa at 50 K), plus the error bar. The nature of these clusters cannot be precisely determined without detailed microscopy, but earlier work shows that dislocation loops with $1/2a\ \langle 111\rangle$ and $a_o\langle 100\rangle$ Burgers vectors can form in Fe–Cr alloys under irradiation (see [7] and references therein). It is important to note that when using a 110-type $g$ vector only half of the $1/2a_0\ \langle 111\rangle$

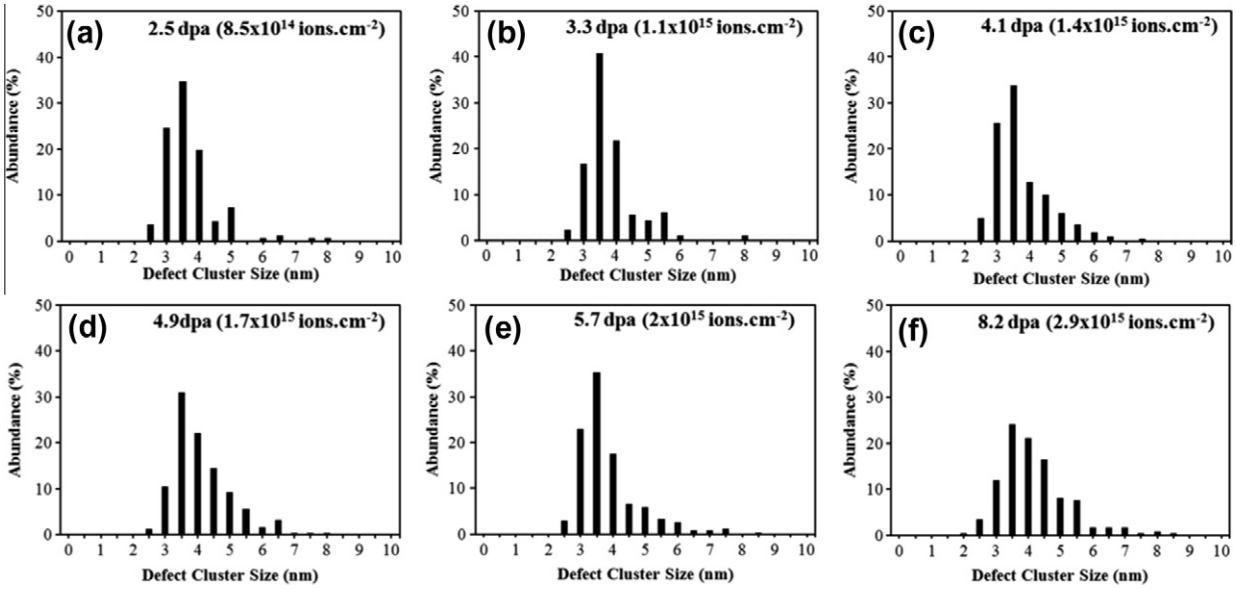


**Fig. 5.** Size distribution of defect clusters in NF616 irradiated with 1 MeV Kr ions at 50 K as a function of dose.

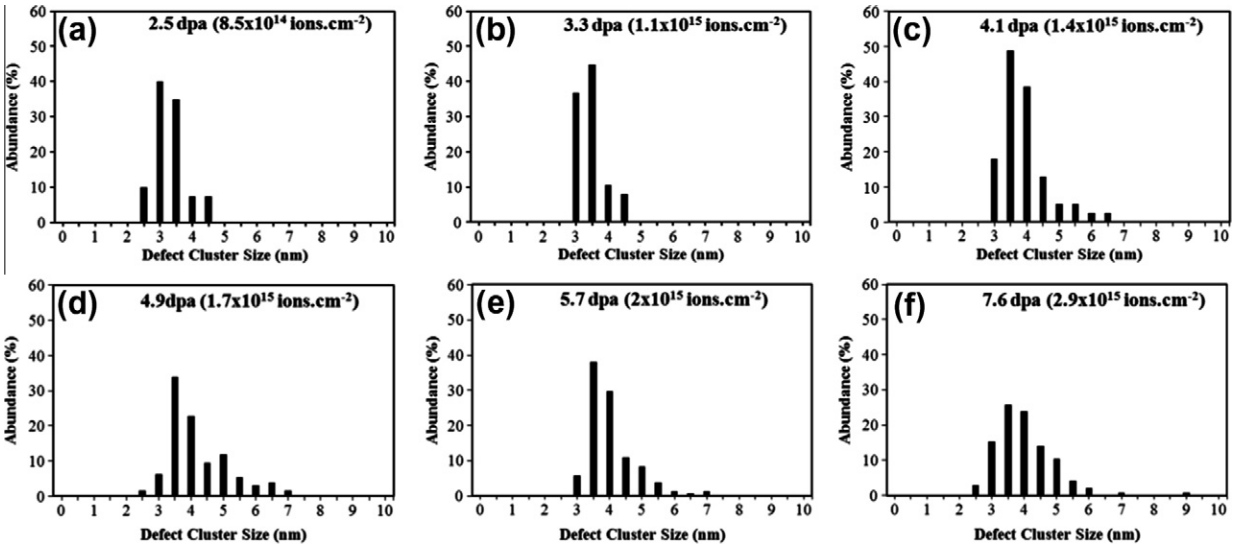


**Fig. 6.** Size distribution of defect clusters in NF616 irradiated with 1 MeV Kr ions at 473 K as a function of dose.

loops and one-third of the $a_0\langle 100\rangle$ loops can be imaged, according to the *g.b* invisibility criterion [8].

It is interesting to note that the saturation density decreases with temperature. Preliminary results indicate that irradiation at intermediate temperatures follows the same trend. Fig. 4b shows the average defect cluster size as a function of dose at 50 K and 473 K. Average defect cluster size values and defect size distributions are shown in Figs. 4b, 5 and 6 only above 2.5 dpa because defect cluster density increases up to 6 dpa, thus improving statistics. The average defect size does not change significantly with dose at 50 K and 473 K, as shown in Fig. 4b.

The defect cluster size distributions are plotted in Figs. 5 (50 K irradiation) and 6 (473 K irradiation) using a bin size of 0.5 nm. The defect cluster size distributions vary little during irradiation, especially after saturation. No significant change is seen between the defect cluster size distributions at 50 K and 473 K.

## 4. Discussion

It is possible to draw some overall conclusions on the irradiation behavior of this material. First, the similarity of the defect size distribution between 50 and 473 K indicates that the role of temperature and cluster mobility is limited in this temperature range. The dynamic observations of defect cluster appearance and disappearance suggests that the creation of defect clusters is caused by a cascade-driven process, in which defect clusters can be formed within cascades or by cascade overlap. Defect density saturation can then occur when the density reaches a level that the probability of a cascade induced shock wave can sweep some of these defect clusters a larger fixed distance and ultimately toward the surface. The fact that the cluster size is constant throughout the irradiation and the same at 50 and 473 K also suggests that the clusters are not influenced by thermal defect migration that would

make them grow or shrink, but rather created and destroyed directly in the cascade events.

The defect cluster density exhibited a non-linear increase at low doses and saturated around ~6 dpa at 50 K and 473 K. It is evident from Fig. 4a that irradiation induced damage started to accumulate at lower doses at 50 K and defect cluster density at 50 K was considerably higher than the defect cluster density at 473 K at low doses and after saturation. Because defect clusters are not observed at low doses at 473 K, it is likely that at those temperatures more cascade overlap is necessary for defect formation. According to this mechanism, TEM-visible defect clusters are expected to form in larger numbers when a critical density of smaller defect clusters is reached (i.e. cascade overlap doses). Production of TEM-visible dislocation loops at cascade overlap doses were reported for ion-irradiated Fe [11], Fe–Cr–C model alloys [12] and an experimental F–M steel, JFMS [13].

The small temperature dependence of microstructure evolution observed in this work is at first glance, puzzling, since point defects of both types are expected to freely migrate at 473 K, while 50 K is in stage 1 for Fe and close pair recovery is the only annihilation mechanism for point defects after cascade cooldown at this temperature [14,15]. It is possible that the solute elements help trap the thermally mobile defects, thus reducing their mobility. The overall observations are, however, consistent with a cascade-driven process which to a first approximation should exhibit less dependence on temperature than a model based on cluster growth by point defect migration. In this case the question is where do the differences observed in defect accumulation (starting dose and final saturation level) between the two temperatures come from. It is possible that the propagation of the shock wave is more efficient at higher substrate temperature, leading to enhanced defect elimination.

## 5. Conclusions

In situ irradiation of NF616 was performed with 1 MeV Kr ions at 50 K and 473 K to investigate microstructure evolution in this alloy. The main results are as follows:

1. Quantitative analysis indicates that defect cluster density increases with dose and saturates at ~6 dpa, at both irradiation temperatures.
2. In situ observations show a dynamic balance between defect creation and annealing, likely caused by the fact that defect cluster formation and destruction is governed by cascade impact.
3. The average size and size distribution of irradiation-induced defect clusters does not change with dose or temperature in this range. This indicates that the effect of temperature is limited in this temperature range.
4. No resolvable loops, voids or irradiation induced precipitates were observed in NF616 irradiated to 8.4 dpa at 50 K and to 7.6 dpa at 473 K. In addition, no significant interaction of the irradiation induced defects with the pre-existing dislocation network or grain boundaries was observed.

## Acknowledgements

This work was funded by the Nuclear Energy Research Initiative Consortium (NERI-C) Award number DE-FG07-07ID14894 from the US Department of Energy. The research conducted in the IVEM-Accelerator facility at Argonne National Laboratory, which is supported as a User Facility by the US Department of Energy, Basic Energy Sciences, under contract W-31-109-ENG-38. We thank Pete Baldo of Argonne National Lab for his help in performing the irradiations. We also thank Djamel Kaoumi, Brian Wirth and Aaron Kohnert for helpful discussions.

## References

[1] A Technology Roadmap for Generation IV Nuclear Energy Systems, US DOE NERAC and Generation IV International Forum, GIF-002-00, 2002.
[2] R.L. Klueh, D.R. Harries, High Chromium Ferritic and Martensitic Steels for Nuclear Applications, American Society for Testing and Materials, West Conshohocken, PA, 2001.
[3] American Society for Testing of Materials, ASTM Standard A335.
[4] R.L. Klueh, A.T. Nelson, J. Nucl. Mater. 371 (2007) 37.
[5] M. Horsten, M.G.E. van Osch, D.S. Gelles, M.L. Hamilton, in: M.L. Hamilton, A.S. Kumar, S.T. Rosinski, M.L. Grossbeck (Eds.), Effects of Irradiation on Materials: 19th International Symposium, ASTM STP 1366, American Society for Testing and Materials, West Conshohocken, PA, 2000, p. 579.
[6] T.R. Allen, L. Tan, J. Gan, G. Gupta, G.S. Was, E.A. Kenik, S. Shutthanandan, S. Thevuthasan, J. Nucl. Mater. 351 (2006) 174.
[7] M.A. Kirk, P.M. Baldo, A.C.Y. Liu, E.A. Ryan, R.C. Birtcher, Z. Yao, Sen Xu, M.L. Jenkins, M. Hernandez-Mayoral, D. Kaoumi, A.T. Motta, Microsc. Res. Tech. 72 (2009) 182.
[8] M.L. Jenkins, M.A. Kirk, Characterisation of Radiation Damage by Transmission Electron Microscopy, Institute of Physics, Philadelphia, PA, 2001.
[9] C.W. Allen, L.L. Funk, E.A. Ryan, Mater. Res. Soc. Symp. Proc. 396 (1996) 641.
[10] J.F. Ziegler, SRIM-2008, v. 2008.40. <http://www.srim.org>.
[11] M.A. Kirk, M. Robertson, J.S. Vetrano, M.L. Jenkins, L.L. Funk, in: F.H. Garner, N.H. Packan, A.S. Kumar (Eds.), Radiation-Induced Changes in Microstructure: 13th International Symposium, ASTM STP 955, American Society for Testing and Materials, Philadelphia, PA, 1987, p. 48.
[12] M.L. Jenkins, Z. Yao, M. Hernández-Mayoral, M.A. Kirk, J. Nucl. Mater. 408 (2011) 194.
[13] H. Fukushima, Y. Shimomura, H. Yoshida, J. Nucl. Mater. 141–143 (1986) 938.
[14] E. Kuramoto, N. Tsukuda, Y. Aono, M. Takenaka, Y. Takano, H. Yoshida, K. Shiraishi, J. Nucl. Mater. 133–134 (1985) 561.
[15] P. Ehrhart, P. Jung, H. Schultz, H. Ullmaier, in: H. Ullmaier (Ed.), Atomic Defects in Metals, Landolt-Börnstein, New Series, Group III, vol. 25, Springer-Verlag, Berlin, 1991.